JOURNAL OF APPLIED PHYSICS **114**, 194508 (2013)

Defect formation in Cu(In,Ga)Se_2 thin films due to the presence of potassium during growth by low temperature co-evaporation process

F. Pianezzi,[a] P. Reinhard, A. Chirilă,[b] S. Nishiwaki, B. Bissig, S. Buecheler, and A. N. Tiwari

Laboratory for Thin Films and Photovoltaics, Empa, Swiss Federal Laboratories for Materials Science and Technology, Ueberlandstrasse 129, 8600 Duebendorf, Switzerland

(Received 23 September 2013; accepted 7 November 2013; published online 21 November 2013)

Doping the Cu(In,Ga)Se_2 (CIGS) absorber layer with alkaline metals is necessary to process high efficiency solar cells. When growth of CIGS solar cells is performed on soda-lime glass (SLG), the alkaline elements naturally diffuse from the substrate into the absorber layer. On the other hand, when CIGS is grown on alkaline free substrates, the alkaline metals have to be added from another source. In the past, Na was believed to be the most important dopant of the alkaline elements, even though K was also observed to diffuse into CIGS from the SLG. Recently, the beneficial effect of a post deposition treatment with KF was pointed out and enabled the production of a 20.4% CIGS solar cell grown at low substrate temperature (<500 °C). However, possible negative effects of the presence or addition of the alkaline impurities during the low temperature growth process were observed for Na, but were not investigated for K so far. In this study, we investigate in detail the role of K on the defect formation in CIGS layers deposited at low temperature on alkaline free polyimide with intentional addition of K during selected time intervals of the CIGS layer growth. By means of admittance spectroscopy and deep level transient spectroscopy, we identify a deep minority carrier trap at around 280 meV below the conduction band E_C in CIGS layers grown with K. Its influence on recombination and minority carrier lifetime in the absorber layer is investigated with external quantum efficiency measurements and time-resolved photoluminescence. Furthermore, to support the experimental findings device simulations were performed using the software SCAPS. © *2013 AIP Publishing LLC*. [http://dx.doi.org/10.1063/1.4832781]

I. INTRODUCTION

Deposition of Cu(In,Ga)Se_2 (CIGS) thin films at low substrate temperature (<500 °C) offers the possibility to produce solar cells on flexible and temperature sensitive substrates such as polyimide (PI). Recently, the high potential of flexible CIGS solar cells on PI for cost effective solar power generation was indicated by reaching a new certified record cell efficiency of 20.4% on laboratory scale,[1] which is at the same level of efficiency as the best devices produced on rigid soda-lime glass (SLG) with a high temperature deposition process (~600 °C) (Ref. 2) or polycrystalline Si-wafer based solar cells.[3] From a manufacturing point of view, flexible substrates have the advantage that roll-to-roll deposition techniques can be used, which enables higher throughput and cost reduction.

A crucial processing step for production of CIGS solar cells is the addition of alkaline material to the CIGS absorber layer. It is well known that a small amount of Na (typically 0.1 at. %) is required in order to achieve high efficiency devices.[4] In the literature, a wealth of changes of the CIGS properties related to Na is reported. While the reports on structural changes in CIGS due to Na are not completely consistent,[5–7] an increase in the p-type conductivity is generally observed.[6,8,9] The latter effect of Na is attributed to either introduction of acceptor defects,[10] elimination of compensating In_{Cu} donors,[11] enhanced oxidation of Se vacancies,[12] or elimination of defects at grain boundaries.[12,13] On the other hand, possible negative effects of sodium—or alkaline metals in general—were usually not considered so far, but it was found that at high Na concentration cell efficiency decreases.[14]

When CIGS solar cells are produced on SLG, Na diffuses during the absorber growth from the substrate through the Mo electrical back contact into the CIGS layer. To produce flexible CIGS solar cells on alkali-free substrates such as metal foils or polyimide,[15–18] various techniques for Na incorporation have been developed, e.g., from a Na doped Mo back contact,[15,19,20] by the deposition of a precursor layer,[21] by co-evaporation,[7,22] by a post deposition treatment (PDT),[6] or from an enamel coating of the substrate.[23]

Up to now, Na is considered to be the most effective alkaline dopant to improve the device performance, although it was observed in several studies that K is also incorporated in CIGS layers grown on SLG.[24,25] Recently, Laemmle *et al.*[26] observed that an intentional addition of K to CIGS by a PDT with KF acts similar as PDT with NaF on the photovoltaic (PV) parameters, i.e., an increase of V_{OC}, FF, and doping density was found due to addition K. On the other hand, we found that PDT with KF leads to a Cu and Ga depleted CIGS surface, which facilitates the diffusion of Cd into the CIGS surface region during the chemical bath deposition (CBD) process of the CdS buffer layer, leading to an

[a]Author to whom correspondence should be addressed. Electronic mail: fabian.pianezzi@empa.ch. Telephone: +41 58 765 61 13

[b]Current address: Flisom AG, Ueberlandstrasse 129, 8600 Duebendorf, Switzerland.

improved junction quality.[1] Similar to the case of doping with Na, there are still many open questions regarding the doping mechanism of K and its overall influence on the final device.

It has previously been shown that Na influences the elemental interdiffusion during the CIGS growth process.[22,27] Moreover, Wuerz *et al.*[23] found that additional K, which diffuses from the K-rich enamel coated steel foil into CIGS during high temperature growth, acts similar as Na: K also hinders elemental interdiffusion and enhances carrier concentration in CIGS layers.

In addition to the presence of alkaline metals, the substrate temperature during CIGS growth has strong influence on the elemental interdiffusion.[17] This effect is clearly visible in the [Ga]/([In] + [Ga]) composition along the CIGS cross-section, forming a much more pronounced double gradient at low substrate temperature as compared to high substrate temperature. The formation of this pronounced compositional gradient throughout the absorber can be compensated by adjusting the deposition rates of the individual metals throughout the process.[17] However, lower substrate temperature will also have effects on an atomic scale (i.e., the occupation of lattice sites) and can result in the formation of higher concentration of anti-site or vacancy defects. Therefore, especially at low substrate temperature, a significant change in the defect formation depending on the amount of alkaline elements present during film growth is expected.

In our laboratoy, high efficiency CIGS solar cells are grown with a modified 3-stage co-evaporation low temperature process with Na added by a PDT method with NaF after the growth of the CIGS layer.[17] In order to investigate the influence of K on the formation of defects and the electronic properties in CIGS grown at low substrate temperature, in this study, we characterized devices with and without co-evaporated KF during the final stage of the CIGS deposition process. As such there are several possibilities for K addition; however, in order to curtail the number of possible effects of K on the electronic properties, KF was added only during the 3rd stage of the deposition process or after CIGS growth.

To identify the energetic position of defects in CIGS, admittance spectroscopy (AS) and deep level transient spectroscopy (DLTS) are performed. Furthermore, the effect of additional defects on the minority carrier lifetime in the CIGS layer is determined with time resolved photoluminescence (TRPL), and the temperature dependent collection of photo-generated charge carriers was investigated by current density-voltage (J-V) measurements in the temperature range from 120 K to 300 K.

II. EXPERIMENTAL DETAILS

CIGS solar cells were produced on Mo coated PI foils with a low substrate temperature (<500 °C) multi-stage co-evaporation process similar to the one described in Ref. 17. In the first set of experiments, we compare the electronic properties of devices without (A1) and with (B1) co-evaporated KF during the entire 3rd stage of the deposition process after reaching the second stoichiometry point, i.e., when the film starts to become Cu-poor again (see Figure 1). After the CIGS growth, the substrate temperature is reduced and a PDT with NaF is applied on both samples A1 and B1.

In a second set of experiments, a comparable amount of KF as in B1 was co-evaporated during selected time intervals of 5 min duration in the 3rd stage. In Figure 1, it is indicated at which stage KF is co-evaporated for the different samples A2-D2. For all samples a PDT with NaF was performed.

All solar cells were completed with a 50 nm thick CdS buffer layer deposited by CBD and an rf-sputtered i-ZnO/ZnO:Al bi-layer front contact of 80 nm and 200 nm thickness, respectively. Finally, Ni/Al grids were deposited.

The PV parameters of the solar cells were measured under simulated standard test conditions (1000 W/m^2, 25 °C). Current density-voltage (J-V) curves were obtained from a Keithley 2400 source meter with four-terminal sensing. External quantum efficiency (EQE) data were measured using a lock-in amplifier and chopped monochromatic light from a halogen lamp in front of a dual grating monochromator. Capacitance-frequency (C-f) measurements were performed with an Agilent E4980A LCR meter. Temperature dependent capacitance measurements, in the temperature range from 120 K to 300 K, were carried out in a cryostat cooled with liquid nitrogen. In the same cryostat, we also performed temperature dependent J-V measurements using a halogen lamp as illumination source.

DLTS measurements were conducted using a Fourier transform 1030 DLTS system from Phys-Tech and a cryostat with liquid nitrogen cooling. Samples were stored in dark prior to measurements for at least 1 h to assure a relaxed state of the device. Capacitance transients were recorded, while the temperature gradually increased from 95 K to 260 K. The reverse bias voltage was set to $U_r = -1.0$ V, and the pulse voltage was $U_p = -0.4$ V such that the pulse height ΔU was 0.6 V with a duration of 10 ms. The period width was set to $T_w = 2$ ms.

TRPL was measured with a near infrared compact fluorescence lifetime spectrometer C12132 by Hamamatsu using a YAG laser with a wavelength of 532 nm. The detection wavelength was set to the photoluminescence maximum.

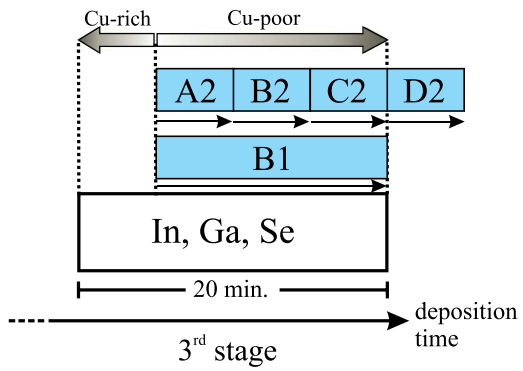

FIG. 1. Schematic drawing of the CIGS deposition procedure during the 3rd stage for the investigated samples B1 and A2-D2. For each sample, KF is evaporated at the stage indicated by the rectangle. For sample D2, KF was added directly after the deposition. Na was added by a PDT with NaF for all samples.

TABLE I. PV parameters (open circuit voltage V_{OC}, short circuit current density J_{SC}, fill factor FF, and efficiency η) of the investigated solar cells. The PV parameters of the best cell on each sample are given. J_{SC} was extracted from EQE measurements.

Sample	V_{OC} (mV)	J_{SC} (mA/cm^2)	FF (%)	η (%)
A1: NaF PDT	670	32.0	77.2	16.6
B1: KF 3rd stage + NaF PDT	678	(30.0[b]) 31.9[a]	76.0	(15.4[b]) 16.4[a]
A2: KF 5–10 min + NaF PDT	680	28.0	64.7	12.3
B2: KF 10–15 min + NaF PDT	678	29.7	75.0	15.1
C2: KF 15–20 min + NaF PDT	711	32.0	72.4	16.5
D2: KF after CIGS growth + NaF PDT	701	33.9	77.7	18.5

[a]With (MgF_2) anti-reflective coating.
[b]Estimated current density/efficiency without AR coating.

III. RESULTS AND DISCUSSION

The PV parameters of the solar cells investigated in this study are listed in Table I. By comparing the PV parameters of A1 and B1, a reduction in the short circuit current density J_{SC} is observed when KF is added during the 3rd stage of CIGS growth (note that for B1 an anti-reflective coating was applied, resulting in a gain in J_{SC} of approximately 2 mA/cm^2). Furthermore, we find that the earlier KF is added during CIGS growth (e.g., sample A2), the lower is J_{SC} of the solar cell. The best cell efficiency was achieved when K was added after CIGS growth, which is partly attributed to a modification of the CIGS surface, as discussed in more detail in Ref. 1.

The reduction in J_{SC} in samples with KF added during the growth process results from poorer collection of long wavelength photons (>600 nm), as shown by the EQE curves in Figure 2. Long wavelength photons are absorbed deeper inside the CIGS layer, possibly outside of the space charge region, such that collection of photo-generated charge carriers strongly depends on their diffusion length L_D in the absorber layer. Thence, it appears likely that in the solar cells, where K is added during CIGS growth (B1 and A2-C2) L_D is reduced.

However, it is difficult to extract the electronic properties, such as defect concentration and charge carrier lifetime in the solar cell, from the PV parameters and EQE alone, because they represent the conjunction of all of these characteristics. Therefore, we used characterization methods which allow accessing defect location/concentration and minority carrier lifetime individually.

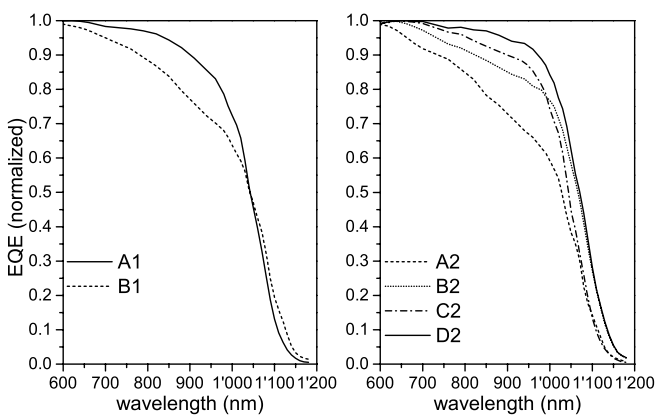

FIG. 2. EQE curves of the investigated solar cells. For better visibility, all curves were normalized. A slight variation in the absorber band gap of approximately 40 meV is observed, which is attributed to differences in Ga content.

A. Formation of defect levels

In order to obtain the defect distribution in the CIGS layer of each sample, we measured their temperature dependent C-f spectra in the range from 120 K to 300 K. First, we compare the C-f spectra of the samples A1 and B1, shown in Figures 3(a) and 3(b), respectively. At low temperature both devices show a step in the capacitance, but at higher temperature sample B1 shows an additional pronounced capacitance step. From these C-f spectra, we calculate the corresponding energy levels of the defects by plotting the scaled derivative $-dC/d\omega^*(\omega/k_BT)$, where $\omega = 2\pi f$ and k_B is the Boltzmann constant, against the energy axis $E_t = k_BT^*\ln(\upsilon_0 T^2/\omega)$. The attempt-to-escape frequency υ_0 was determined from the slope of an Arrhenius plot of the inflection frequency against 1/T (see Ref. 28). The resulting defect spectra are shown in Figures 3(c) and 3(d).

The shallow level below 100 meV, which is observed in both devices, is attributed to the N1 signal. The origin of this signal is still debated in the research community[29–31] and shall not be discussed in more detail in this paper.

In the following, we focus mainly on the deeper defect located at around 280 meV, which we observe in the device with additional co-evaporated KF during the 3rd stage but not in the device without KF (NaF PDT only).

In the second set of samples (A2-C2) where KF was added at selected time intervals during the 3rd stage of the CIGS deposition process, we also observe the deep defect level at 280 meV, as shown in Figures 4(a)–4(c). Only in the sample D2 where KF was added after the CIGS growth process, the deep defect is not observed (Figure 4(d)).

From Figures 3 and 4, we conclude that the presence of K during CIGS growth strongly influences the concentration of the deep defect level at 280 meV. Furthermore, addition of K after CIGS growth does not lead to the formation of this defect level (at least not in a concentration high enough to be measured with AS).

B. Identification of the defect position

From the AS measurements presented in Sec. III A, it is not possible to assign the deep defect level at 280 meV to a majority or a minority carrier trap. According to Lang, the

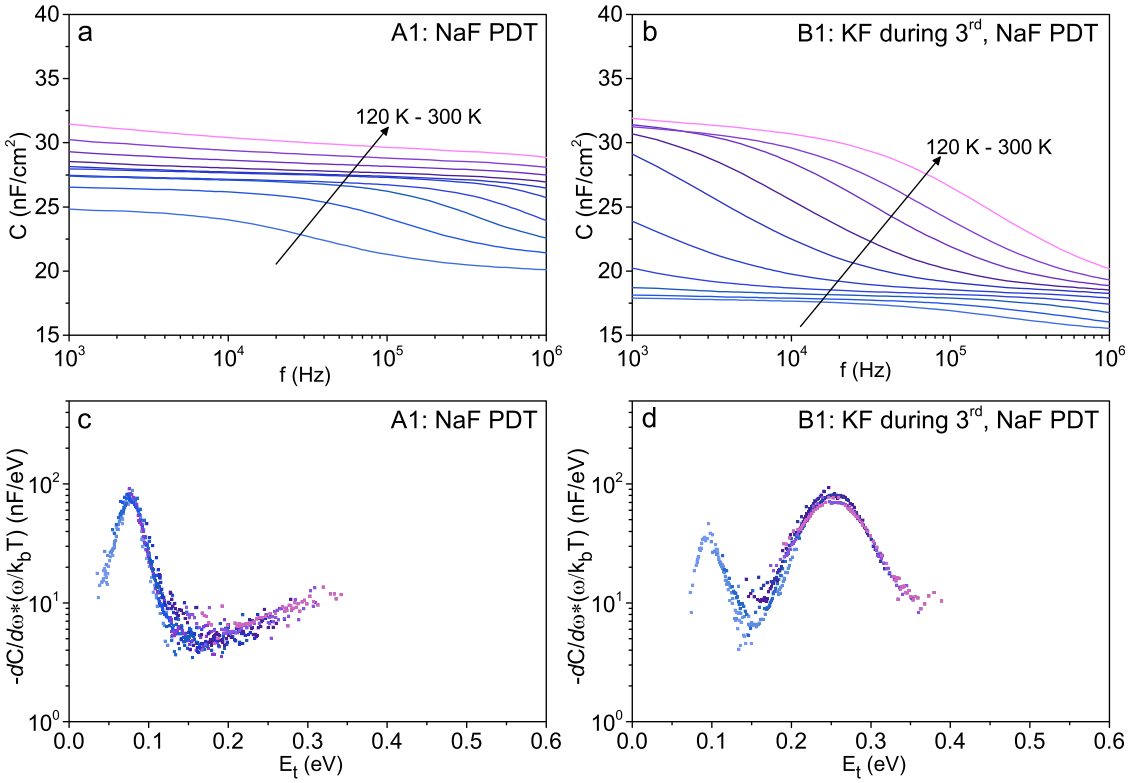

FIG. 3. C-f and defect spectra of a CIGS solar cell with NaF PDT only ((a) and (c)) and a CIGS solar cell with additional KF co-evaporated during the 3rd stage ((b) and (d)).

sign of the capacitance transient in DLTS indicates whether a majority or a minority carrier trap is present.[32] Therefore, we performed DLTS measurements on samples B2 and D2, and the resulting spectra are shown in Figures 5(a) and 5(b), respectively. In sample B2, we observe two signals (E_1 and E_2). Both of them show positive capacitance transients and can therefore be identified as minority carrier traps. The energetic position represents in this case the distance of the

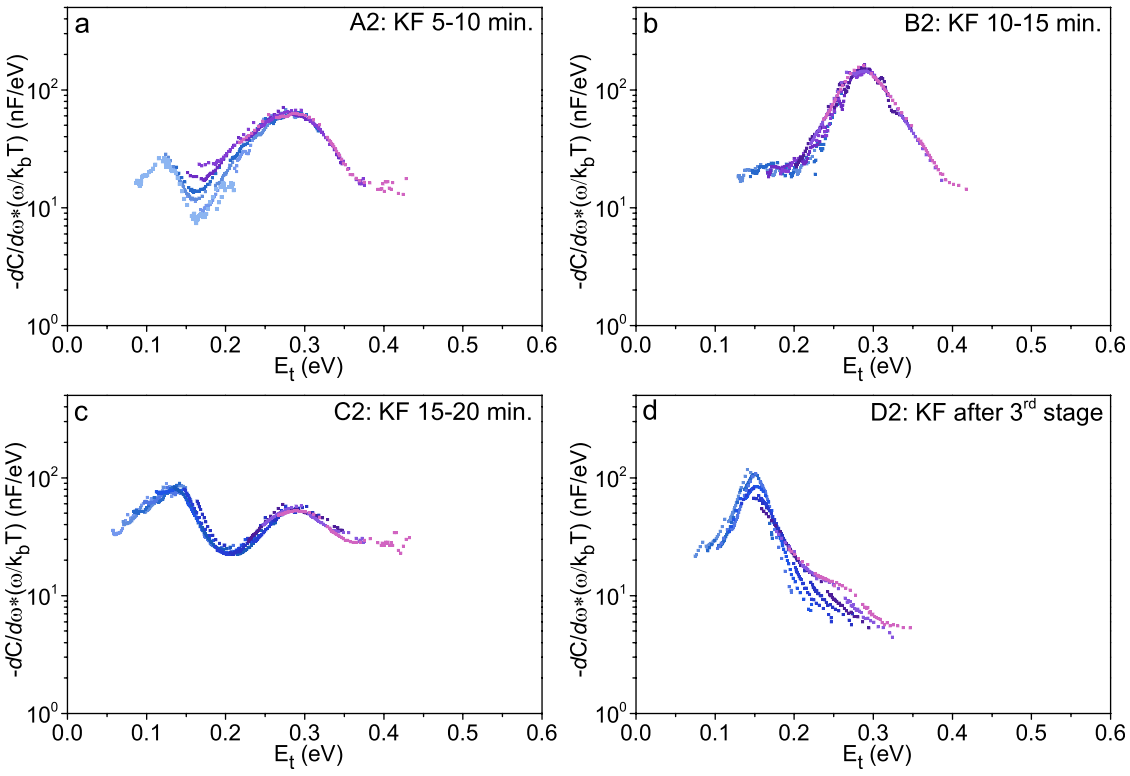

FIG. 4. Defect spectrum of samples A2-D2 with KF added from 5 to 10 min (a), from 10 to 15 min (b), from 15 to 20 min (c), during the 3rd stage as well as directly after the end of the 3rd stage (d).

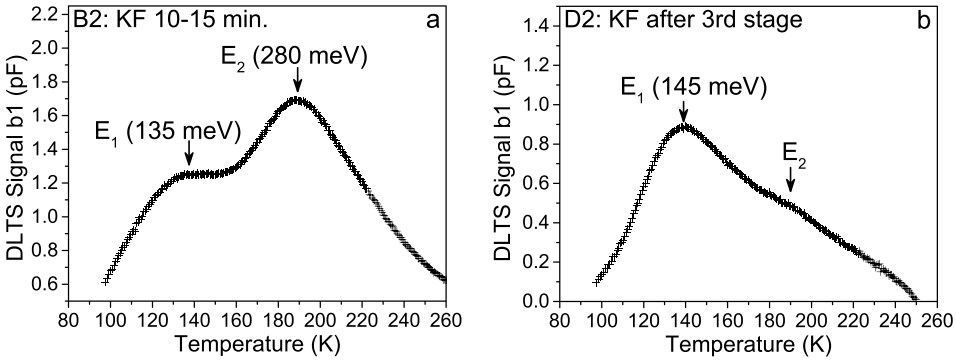

FIG. 5. DLTS spectrum of sample B2 (a) and sample D2 (b) from 95 K to 260 K. Two distinct positive peaks (indicated by E_1 and E_2) are visible in the spectrum of sample B2. Due to the weak intensity of signal E_2 in sample D2, it was not possible to determine its energy exactly. The sign of the DLTS signal indicates that the observed levels correspond to minority carrier traps in the CIGS absorber layer.

defect level to the conduction band. In sample D2, the signal E_1 at 140 K is also present, and at higher temperature a weak signature of the defect E_2 is observed. The calculated energies of the defects are given in Figure 5(a), and they are in accordance with the defect levels observed in the AS measurements presented above.

Again, the signal E_1 at low temperature (140 K) is attributed to the N1 level, for both devices. The N1 signal was previously identified as a minority carrier trap.[33] The DLTS signal at 190 K corresponds to the deep defect at 280 meV shown in Figure 4. The fact that the DLTS signal at 190 K did not completely disappear for sample D2 shows that the defect level is still present in the device but at much lower concentration.

C. Influence of the deep defect level on minority carrier lifetime

The deep defect level observed at around 280 meV below E_C can capture and re-emit electrons, as shown by the DLTS measurements in Sec. III B. On the other hand, a captured electron can also recombine with a hole, which is directly related to the minority carrier lifetime in the CIGS layer and the collection of photo-generated charge carriers (cf. Figure 2). A schematic diagram of the different processes is shown in Figure 6(a).

We used room temperature TRPL measurements to determine the influence of the deep defect level on the minority carrier lifetime in the CIGS layer. The measurements were performed on completed solar cells. In Figure 6(b), the time evolution of the PL signal for the samples A2-D2 is shown together with the calculated lifetime τ from an exponential fit.

We observe that the minority carrier lifetime is smaller in devices in which K was present during CIGS growth (samples A2-C2). Therefore, we conclude that the minority carrier trap at 280 meV below E_C, which was observed in the samples A2-C2, contributes to the recombination in the CIGS layer. This leads to the reduced collection of charge carriers generated by long wavelength photons (cf. Figure 2) because the minority carrier diffusion length $L_D = \sqrt{D\tau}$ (D is the minority carrier diffusivity) in the absorber layer becomes smaller.

Furthermore, the earlier K is added during growth, the lower is the minority carrier lifetime. This suggests that the remaining time until finishing CIGS growth after addition of K is relevant for the electronic properties of the device.

D. Temperature dependence of the photocurrent

The defect level at 280 meV is relatively close to E_C, and therefore it is not a very effective recombination centre at room temperature, because the emission rate e_n of trapped electrons, which is given by

$$e_n = \sigma_n v_{th} N_C \cdot \exp\left(-\frac{E_C - E_t}{k_B T}\right), \tag{1}$$

(where σ_n is the capture cross section for electrons, v_{th} is the thermal velocity of electrons, N_C is the density of states in

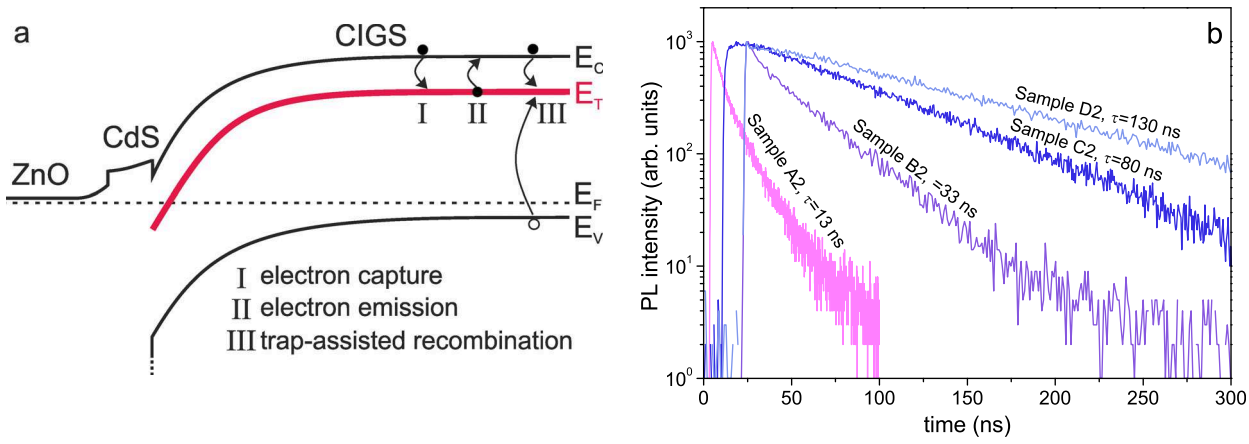

FIG. 6. (a) Schematic illustration of the energy band diagram of a CIGS solar cell and the electron capture/emission, as well as trap-assisted recombination, are shown. In (b) the time evolution of the room temperature PL signal of the A2-D2 is shown.

the conduction band, and E_t is the energy of the defect level) is high such that it is likely that trapped electrons are re-emitted from the defect before recombining with holes from the valance band E_V. Nevertheless, we observed a decrease in the minority carrier lifetime and reduced collection of photo-generated charge carriers in samples B1 and A2-C2, which shows that some of the excited electrons do indeed recombine, even at room temperature.

Because the emission rate of trapped electrons decreases with temperature (the prefactor $\sigma_n v_{th} N_D$ in Eq. (1) is $\propto T^2$, see, e.g., Ref. 34), it is possible to observe the recombination via this defect in the photocurrent by cooling the device to low temperature. In Figures 7(a) and 7(b), we show temperature dependent J-V measurements under illumination of the samples B1 (samples A2-C2 behave similarly) and A1, respectively. At low temperature J_{SC} is strongly reduced in sample B1 by approximately 10 mA/cm^2, because part of the photo-generated charge carriers recombined before being collected by the electric field of the pn-junction. In contrast, sample A1, as well as D2 (not shown), did not exhibit such a strong temperature dependence of the photo-current density in the accessible temperature range (Figure 7(b)).

To verify that the defect level at 280 meV is indeed responsible for the reduced photocurrent at low temperature, we performed device simulations using the software SCAPS.[35] For the model, the parameters of the individual layers were adapted from Ref. 17. In addition, a defect level at 280 meV below E_C with a concentration of 2×10^{16} cm^{-3}, a capture cross-section for electrons of 10^{-16} cm^{-2}, and a capture cross-section for holes of 10^{-18} cm^{-2}, was included. The resulting J-V curves of the simulation are shown in Figure 7(c) and agree very well with the measurement in Figure 7(a).

To show that the observed temperature dependence of the photocurrent is typical for a minority carrier trap at around 280 meV, we also varied the position of the defect level in our simulation. The temperature dependence of the J_{SC} for different positions of the defect is shown in Figure 7(d).

For defects close to the conduction band (0.15 eV below E_C), the temperature where J_{SC} starts to decrease is moved to lower values because the emission rate of trapped electrons is high even at a temperature of 150 K. As expected, for defects close to mid-gap position (0.55 eV below E_C), the photocurrent is also reduced at room temperature because recombination rate via this defect is high. For defect levels in between these two extremes (e.g., 250 meV below E_C), we can observe a strong temperature dependence of the J_{SC} below approximately 200 K, as shown in Figure 7(c).

E. Origin of the deep defect level

Our results show that the presence of K during CIGS growth at low temperature leads to the formation of a deep

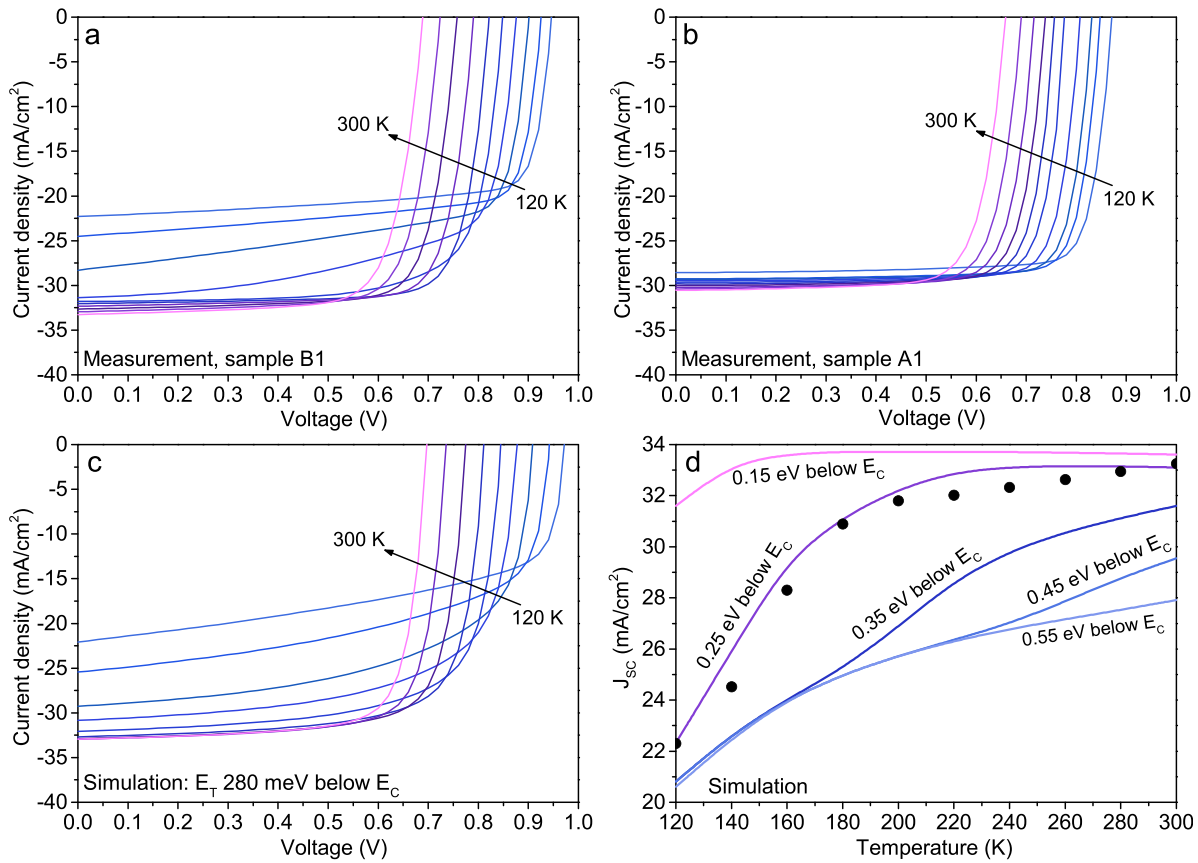

FIG. 7. Measured (a) and (b) temperature dependence of the J-V curves of the solar cells B1 and A1, respectively. Note that the measurements were performed with a halogen lamp as illumination source, such that the measured photocurrent density may deviate from the values given in table I (c) SCAPS simulation of the temperature dependent J-V curves of sample B1. In (d) a SCAPS simulation of the temperature dependence of the J_{SC} for different energetic positions of the defect level in the band gap is given. Circles represent measured J_{SC} of sample B1.

defect at 280 meV below the conduction band, which is not observed in devices without K. We suggest that two scenarios are possible: (i) K introduces a point defect such as $K_{In,Ga}$ or (ii) K influences elemental interdiffusion, resulting in higher concentration of intrinsic defects. To the best of our knowledge there exists currently no theoretical study on either possibility. Up to now, formation energies of point defects in $CuInSe_2$ and related materials were calculated only for Na but not for K.[11,36]

Experimentally, other authors also observed such a deep level in CIGS grown on SLG by transient photo-capacitance (TPC) measurements.[37,38] They found that its position at 0.8 eV above E_V is independent of the Ga content, such that it may become an effective recombination center in CIGS layers with high Ga content because the energy $(E_C - E_T)$ increases (cf. Figure 7(c)).

In a recent theoretical study based on hybrid density functional theory by Pohl and Albe, it was concluded that the deep defect that we observe at around 0.8 eV above the E_V might origin from deep $Cu_{In,Ga}$ (-1/-2) charge transition levels, which have energies of 0.62 eV and 0.75 eV above E_V in $CuInSe_2$ and $CuGaSe_2$, respectively.[39] On the other hand, other authors concluded that Se-related defects rather than Cu- or In-related defects form charge transition levels within the band gap.[40] Earlier calculations performed by Lany and Zunger suggested that the $(V_{Se}$-$V_{Cu})$ defect complex is responsible for this level.[41] Currently, we cannot judge with certainty which point-defect (complex) is responsible for the observed defect level. Detailed investigation of elemental interdiffusion as well as calculation of defect formation energies in dependence of the presence of K and the calculation of possible charge transition levels inside the CIGS band gap of K-related point defects (e.g., $K_{In,Ga}$) could help to identify its origin.

IV. CONCLUSIONS

In this work, we investigated the formation of defects in CIGS layers depending on the presence of K during the low temperature growth process. K was added by co-evaporation from a KF source. Using AS and DLTS, we found that the presence of K during the final stage of the CIGS growth leads to the formation of a deep defect level approximately 280 meV below the conduction band. Therefore, devices in which K was present during growth showed reduced minority carrier lifetime, and poorer collection of charge carriers generated by long wavelength photons. Furthermore, strongly temperature dependent collection of photogenerated charge carriers is observed, which is explained by an increasing recombination rate via this defect at lower temperature of the device.

Currently, it is not possible to unambiguously attribute the observed defect to any of the possible point defects in CIGS. However, we believe that our results could help to identify its origin by studying elemental interdiffusion and formation energies of point defects in dependence of the presence of K.

Finally, our results suggest that growth of CIGS absorber layers, especially with high Ga content and low substrate temperature, should be performed under conditions without K, because, according to the previous studies,[38] the observed defect level is at fixed position of approximately 0.8 eV above the valence band and becomes a deep trap when E_C is lifted to higher energy. In this respect, growth of Ga rich CIGS absorber layers at low substrate temperature should be performed on alkaline free substrates, while Na and K could be introduced after CIGS growth.

ACKNOWLEDGMENTS

The Integrated Systems Laboratory, ETH Zurich, is gratefully acknowledged for giving access to the DLTS measurement setup and we would like to thank Hamamatsu for providing the TRPL measurement setup.

[1]A. Chirilă, R. Reinhard, F. Pianezzi, P. Bloesch, A. R. Uhl, C. Fella, L. Kranz, D. Keller, C. Gretener, H. Hagendorfer, D. Jaeger, R. Erni, S. Nishiwaki, S. Buecheler, and A. N. Tiwari, "Potassium-induced surface modification of $Cu(In,Ga)Se_2$ thin films for high-efficiency solar cells," Nature Mater. **12**, 1107 (2013).
[2]P. Jackson, D. Hariskos, E. Lotter, S. Paetel, R. Wuerz, R. Menner, W. Wischmann, and M. Powalla, Prog. Photovoltaics **19**, 894 (2011).
[3]O. Schultz, S. W. Glunz, and G. P. Willeke, Prog. Photovoltaics **12**, 553 (2004).
[4]D. Rudmann, D. Brémaud, A. F. da Cunha, G. Bilger, A. Strohm, M. Kaelin, H. Zogg, and A. N. Tiwari, Thin Solid Films **480–481**, 55 (2005).
[5]K. Granath, M. Bodegård, and L. Stolt, Sol. Energy Mater. Sol. Cells **60**, 279 (2000).
[6]D. Rudmann, A. F. da Cunha, M. Kaelin, F. Kurdesau, H. Zogg, A. N. Tiwari, and G. Bilger, Appl. Phys. Lett. **84**, 1129 (2004).
[7]D. Rudmann, G. Bilger, M. Kaelin, F. J. Haug, H. Zogg, and A. N. Tiwari, Thin Solid Films **431–432**, 37 (2003).
[8]T. Nakada, D. Iga, H. Ohbo, and A. Kunioka, Jpn. J. Appl. Phys., Part 1 **36**, 732 (1997).
[9]M. Lammer, U. Klemm, and M. Powalla, Thin Solid Films **387**, 33 (2001).
[10]D. W. Niles, K. Ramanathan, F. Hasoon, R. Noufi, B. J. Tielsch, and J. E. Fulghum, J. Vac. Sci. Technol. A **15**, 3044 (1997).
[11]S.-H. Wei, S. B. Zhang, and A. Zunger, J. Appl. Phys. **85**, 7214 (1999).
[12]L. Kronik, D. Cahen, and H.-W. Schock, Adv. Mater. **10**, 31 (1998).
[13]E. S. Mungan, W. Xufeng, and M. A. Alam, IEEE J. Photovoltaics **3**, 451 (2013).
[14]A. Rockett, J. S. Britt, T. Gillespie, C. Marshall, M. M. Al Jassim, F. Hasoon, R. Matson, and B. Basol, Thin Solid Films **372**, 212 (2000).
[15]R. Wuerz, A. Eicke, F. Kessler, P. Rogin, and O. Yazdani-Assl, Thin Solid Films **519**, 7268 (2011).
[16]R. Wuerz, A. Eicke, M. Frankenfeld, F. Kessler, M. Powalla, P. Rogin, and O. Yazdani-Assl, Thin Solid Films **517**, 2415 (2009).
[17]A. Chirilă, S. Buecheler, F. Pianezzi, P. Bloesch, C. Gretener, A. R. Uhl, C. Fella, L. Kranz, J. Perrenoud, S. Seyrling, R. Verma, S. Nishiwaki, Y. E. Romanyuk, G. Bilger, and A. N. Tiwari, Nature Mater. **10**, 857 (2011).
[18]F. Pianezzi, A. Chirilă, P. Blösch, S. Seyrling, S. Buecheler, L. Kranz, C. Fella, and A. N. Tiwari, Prog. Photovoltaics **20**, 253 (2012).
[19]P. Blösch, S. Nishiwaki, A. Chirilă, L. Kranz, C. Fella, F. Pianezzi, C. Adelhelm, E. Franzke, S. Buecheler, and A. N. Tiwari, Thin Solid Films **535**, 214 (2013).
[20]J. H. Yun, K. H. Kim, M. S. Kim, B. T. Ahn, S. J. Ahn, J. C. Lee, and K. H. Yoon, Thin Solid Films **515**, 5876 (2007).
[21]R. Caballero, C. A. Kaufmann, T. Eisenbarth, A. Grimm, I. Lauermann, T. Unold, R. Klenk, and H.-W. Schock, Appl. Phys. Lett. **96**, 092104 (2010).
[22]D. Guettler, A. Chirila, S. Seyrling, P. Bloesch, S. Buecheler, X. Fontane, V. Izquierdo-Roca, L. Calvo-Barrio, A. Perez-Rodriguez, J. R. Morante, A. Eicke, and A. N. Tiwari, in *Proceedings of the Conference Record of 35th Photovoltaic Specialists Conference 2010, Honolulu, Hawai, 20–25 June*, 2010, pp. 3420–3424.
[23]R. Wuerz, A. Eicke, F. Kessler, S. Paetel, S. Efimenko, and C. Schlegel, Sol. Energy Mater. Sol. Cells **100**, 132 (2012).

[24]P. Jackson, R. Würz, U. Rau, J. Mattheis, M. Kurth, T. Schlötzer, G. Bilger, and J. H. Werner, Prog. Photovoltaics **15**, 507 (2007).
[25]O. Cojocaru-Mirédin, P.-P. Choi, D. Abou-Ras, S. S. Schmidt, R. Caballero, and D. Raabe, IEEE J. Photovoltaics **1**, 207 (2011).
[26]A. Laemmle, R. Wuerz, and M. Powalla, Phys. Status Solidi (RRL) **7**, 631 (2013).
[27]O. Lundberg, J. Lu, A. Rockett, M. Edoff, and L. Stolt, J. Phys. Chem. Solids **64**, 1499 (2003).
[28]T. Walter, R. Herberholz, C. Müller, and H.-W. Schock, J. Appl. Phys. **80**, 4411 (1996).
[29]U. Reislöhner, H. Metzner, and C. Ronning, Phys. Rev. Lett. **104**, 226403 (2010).
[30]P. Zabierowski, K. Stankiewicz, A. Donmez, F. Couzinie-Devy, and N. Barreau, Thin Solid Films **519**, 7485 (2011).
[31]T. Eisenbarth, T. Unold, R. Caballero, C. A. Kaufmann, and H.-W. Schock, J. Appl. Phys. **107**, 034509 (2010).
[32]D. V. Lang, J. Appl. Phys. **45**, 3023 (1974).
[33]R. Herberholz, M. Igalson, and H. W. Schock, J. Appl. Phys. **83**, 318 (1998).
[34]*Advanced Characterization Techniques for Thin Film Solar Cells*, edited by U. Rau, D. Abou-Ras, and T. Kirchartz (WILEY-VCH Verlag GmbH & Co, Weinheim, Germany, 2011).
[35]M. Burgelman, P. Nollet, and S. Degrave, Thin Solid Films **361–362**, 527 (2000).
[36]L. E. Oikkonen, M. G. Ganchenkova, A. P. Seitsonen, and R. M. Nieminen, J. Appl. Phys. **114**, 083503 (2013).
[37]T. Sakurai, H. Uehigashi, M. M. Islam, T. Miyazaki, S. Ishizuka, K. Sakurai, A. Yamada, K. Matsubara, S. Niki, and K. Akimoto, Thin Solid Films **517**, 2403 (2009).
[38]J. T. Heath, J. D. Cohen, W. N. Shafarman, D. X. Liao, and A. A. Rockett, Appl. Phys. Lett. **80**, 4540 (2002).
[39]J. Pohl and K. Albe, Phys. Rev. B **87**, 245203 (2013).
[40]L. E. Oikkonen, M. G. Ganchenkova, A. P. Seitsonen, and R. M. Nieminen, Phys. Rev. B **86**, 165115 (2012).
[41]S. Lany and A. Zunger, J. Appl. Phys. **100**, 113725 (2006).